$O(^3P) + C_2H_4$ Potential Energy Surface: Study at the Multireference Level†

Aaron C. West,‡ Joshua S. Kretchmer,§ Bernhard Sellner,|| Kyoyeon Park,⊥ William L. Hase,⊥ Hans Lischka,||,# and Theresa L. Windus*,‡

Department of Chemistry, Iowa State University, Ames, Iowa 50011, Department of Chemistry, University of California at Berkeley, Berkeley, California 94720, Institute for Theoretical Chemistry, University of Vienna, Waehringerstrasse 17, A-1090 Vienna, Austria, Department of Chemistry and Biochemistry, Texas Tech University, Memorial Circle & Boston, Lubbock, Texas 79409-1061, and Institute of Organic Chemistry and Biochemistry, Academy of Sciences of the Czech Republic, Flemingovo nam. 2, CZ-16610 Prague 6, Czech Republic

Received: May 29, 2009; Revised Manuscript Received: September 30, 2009

The $O(^3P) + C_2H_4$ reaction provides a crucial, initial understanding of hydrocarbon combustion. In this work, the lowest-lying triplet potential energy surface is extensively explored at the multiconfiguration self-consistent field (MCSCF) and MRMP2 levels with a preliminary surface crossing investigation; and in cases that additional dynamical correlation is necessary, MR-AQCC stationary points are also determined. In particular, a careful determination of the active space along the intrinsic reaction pathway is necessary; and in some cases, more than one active space must be explored for computational feasibility. The resulting triplet potential energy surface geometries mostly agree with geometries from methods using single determinant references. However, although the selected multireference methods lead to energetics that agree well, only qualitative agreement was found with the energetics from the single determinant reference methods. Challenges and areas of further exploration are discussed.

Introduction

The O + ethylene reaction not only serves as an important intermediate in the combustion of most fuels[1] but also provides insight into possible reaction mechanisms involved in the low-Earth orbit erosion (LEO) of space vehicles. However, understanding these reaction schemes is a challenge to both computation and experiment. Several low-pressure, crossed-molecular-beam experiments (CMBEs) have been performed for this reaction with only the most recent ones discussed here (the reader is referred to references in these works for early experiments[2−4]). Casavecchia et al. used a low-energy, tunable, soft ionization mass spectrometer to reduce the background of dissociative ionization that previous CMBEs experienced and calculated the branching ratios of five competing channels. In particular, this method indirectly characterized several new channels, which include the radical CHO channel.[2] Su et al. used step-scan, time-resolved Fourier transform infrared (FTIR) to characterize the formaldehyde channel for reactions of $O(^3P)$ with several alkenes.[3,4] Lee et al. used a CMBE with single-photon ionization to directly observe radical CHO and several other channels.[4]

Under collision-free conditions from 287 to 2000 K, the most dominant channels comprise the species $CH_2CHO + H$, $CH_3 + CHO$, and $CH_2 + H_2CO$.[5] To pass through these three channels, the reaction path must include the ketocarbene that directly follows from oxygen addition to ethylene. From this ketocarbene triplet biradical, the CH_2CHO and H_2CO channels each involve only one appropriate decomposition pathway on the triplet surface. However, without hyperthermal conditions, the CHO channel faces a large barrier on the triplet surface and will involve an intersystem crossing (ISC) to the singlet surface, a hydrogen shift, and then the appropriate decomposition. Overall product distributions actually remain pressure-independent over a temperature range of 287−2000 K and a pressure range of 0.007−1 atm.[5] In fact, Nguyen et al.[5] have shown that adduct collisional stabilization remains negligible even at 100 atm and ∼1500 K where <10% triplet adduct stabilization occurs. Thus, temperature primarily controls product distributions under these kinds of conditions. For instance, the product percents of the three channels at 298 K are theoretically and experimentally 40 ± 10, 50 ± 10, and 10 ± 5, whereas at 2000 K theoretically available values are 18.5, 36.9, and 29.1.[5] Of course, as the temperature varies, all channel product distributions change.

This reaction also presents a theoretical challenge all on its own. Several theoretical studies characterized only static, stationary points,[6,7] but other examinations considered important reaction pathways.[8−10] Some lower level studies led to important qualitative reaction schemes.[7,8] However, Nguyen et al.[5] and Schatz et al.[5,11] more generally examined this potential energy surface. From all the above theoretical studies, major highlights include (1) the initial hydrogen abstraction channel can compete with the oxygen addition channel only in hyperthermal regions, (2) the oxygen asymmetrically adds to one of ethylene's carbons, and (3) the triplet biradical complex rapidly decomposes via the $CH_2CHO + H$ channel. The Schatz and Nguyen studies provide excellent, general O + ethylene surface explorations; however, these studies have discrepancies. For instance, Schatz et al. had difficulty locating some stationary points with the UB3LYP theory level, and some energy barriers differ between these two studies by up to ∼7 kcal/mol. These issues will obviously affect differences in dynamics between the two studies. At low temperatures for this system, large portions of

† Part of the "Russell M. Pitzer Festschrift".

* Corresponding author. Phone: 515-294-6134. Fax: 515-294-0105. E-mail: twindus@iastate.edu.

‡ Iowa State University.

§ University of California at Berkeley.

|| University of Vienna.

⊥ Texas Tech University.

Academy of Sciences of the Czech Republic.

10.1021/jp905070z CCC: $40.75 © 2009 American Chemical Society
Published on Web 10/13/2009

the potential will remain inaccessible, and so these discrepancies will not be as significant. However, under LEO conditions, higher temperatures access more of the electronic surface. Thus, studies of O + ethylene along with more complex combustion reactions require an accurate surface in hyperthermal regions. Whereas Nguyen examined some of the critical biradicals with multiconfigurational methods, most species were examined with the single determinant based methods G3,[12] CBS-QB3,[13] and G2M(CC,MP2)[14] as well as MRCI.[15,16] These methods provided single-point energies on B3LYP/6-311++G(3df,2p) optimized geometries. Nguyen et al. averaged the single-determinant-based results to give average barriers for both energetics and dynamics. Since both surfaces have many reaction pathways with radical character throughout, these single determinant methods may not give proper wave functions or barriers in certain cases.

In the O + ethylene reaction, both the lowest-lying triplet and singlet play important roles. However, this study mostly examines the lowest triplet surface; future studies will analogously examine the lowest singlet surface. The important lowest-lying triplet reaction pathways are listed below. Nguyen's study contains pathways 1 − 9, but pathway 10 is not located in that study.

$$\bullet\bullet O + C_2H_4 \rightarrow \bullet CH_2CH_2O\bullet \quad (1)$$

$$\bullet\bullet O + C_2H_4 \rightarrow \bullet OH + \bullet C_2H_3 \quad (2)$$

$$\bullet CH_2CH_2O\bullet \rightarrow \bullet CH_2CHO + \bullet H \quad (3)$$

$$\bullet CH_2CH_2O\bullet \rightarrow \bullet\bullet CH_2 + H_2CO \quad (4)$$

$$\bullet CH_2CH_2O\bullet \rightarrow CH_3\bullet CHO\bullet \quad (5)$$

$$\bullet CH_2CH_2O\bullet \rightarrow \bullet CH_2\bullet CHOH \quad (6)$$

$$CH_3\bullet CHO\bullet \rightarrow \bullet CH_3 + \bullet CHO \quad (7)$$

$$CH_3\bullet CHO\bullet \rightarrow \bullet CH_3\bullet CO + \bullet H \quad (8)$$

$$CH_3\bullet CHO\bullet \rightarrow \bullet H + \bullet CH_2CHO \quad (9)$$

$$CH_3\bullet CHO\bullet \rightarrow \bullet CH_2\bullet CHOH \quad (10)$$

The rest of the paper is organized as follows: The next section outlines the Methods and includes the choice of active spaces. The Results and Discussion summarizes the active space investigation, system energetics, and initial findings on relevant surface crossings. Finally, the Conclusion discusses findings relative to Nguyen et al. and summarizes overall results.

Methods

Results from calculations at the MCSCF and MRMP2 levels in this paper were performed with the GAMESS software.[17] To recover the majority of the static correlation, all calculations were carried out with a complete active space self-consistent field (CASSCF)[18−20] level of theory using the aug-cc-pVTZ[21] basis set (the choice of the aug-cc-pVTZ is justified in the discussion of pathway 1). Because of large complete active space (CAS) sizes and biradical species in this study, the determinant-based method[22] and the full Newton−Raphson (FULLNR) converger with augmented Hessian technique[23−25] were used to provide solutions. Restricted Hartree−Fock (RHF) or restricted open shell Hartree−Fock (ROHF) calculations with modified valence orbitals[26] provided good MCSCF starting orbitals in most situations. However, Boys localization[27] provided better starting orbitals in difficult cases. To aid in the convergence of the CASSCF and to prevent convergence to any undesired higher spin states, geometry optimization calculations utilized three configuration interaction (CI) states.

CASSCF stationary point searches for species in the reactions above employed analytical gradients and double differenced, numerical Hessians to characterize the stationary points as first-order maxima or minima on the potential energy surface and to obtain zero-point energies (ZPE) and frequencies. At each of the triplet stationary points, 5−10 CI states were calculated to check that the lowest electronic state was attained and to obtain a qualitative picture of the location of the nearest excited states. In addition, 5−10 CI states were also found, starting from the singlet wave function density at the triplet stationary point geometries, to obtain an initial understanding of energetically close-lying states. Since any close-lying, excited state densities may differ from the density of the lowest-lying state of identical spin, a state-averaged CASSCF study could provide a more accurate picture of such states. However, such a study is outside the scope of the current paper.

Intrinsic reaction coordinate (IRC) calculations identified reactants and products associated with each transition state. The second-order, Gonzalez-Schlegel (GS2) method[28] provided a robust, steepest descent path in mass-weighted coordinates from the transition state to the minima. Near the transition state, all IRC runs started with a step size of 0.05 bohr × sqrt(amu) for 10 steps. This many initial small steps sufficiently ensured smooth IRCs if the FULLNR converger led to a consistent active space. Then, all IRC runs completed with a step size of 0.15 bohr × sqrt(amu).

Once a reaction path was located, single-state, second-order multireference Møller−Plesset perturbation (MRMP2)[29,30] single-point energies using the aug-cc-pVTZ basis set were performed along the IRC to recover the majority of the dynamic correlation. In reaction pathways where a second-order perturbation theory might not be sufficient to account for the dynamical correlation, stationary points and energetics were also obtained with multireference average quadratic couple cluster (MR-AQCC)[31] using COLUMBUS.[32−34] This method not only recovers more dynamical correlation but also has less sensitivity to the choice of active space. Moreover, this method has the advantage that analytic gradients are available, allowing geometry optimizations at a fully correlated level.[35] Force constants are computed by means of finite differences of energy gradients. Due to the computational expense of these calculations, geometries were determined with an (8, 6) active space using the cc-pVDZ[21] basis for H and the cc-pVTZ[21] basis without *f* functions for C and O (referred to as BS1 in this work). In this particular system, the MR-AQCC results show sensitivity to the basis set; so several single-point energies using different basis sets were used: cc-pVDZ on H and cc-pVTZ on C and O (referred to as BS2) and cc-pVTZ on H and aug-cc-pVTZ on C and O (referred to as BS3).

Of course, the choice of the active space is of critical importance. Several active space sizes were examined for each reaction pathway; Table 1 gives only the most appropriate sizes. However, other somewhat appropriate sizes will be discussed as needed in the sections below. At the moment, MRMP2

TABLE 1: Description of the Main CAS Sizes Used for Each Reaction Pathway[a]

reaction pathway	active space	in−out correlation	description
1	(6, 6)	N	CCσ, CCπ, biradical (2 O2p) → CCσ, COσ, biradical (far C2p, O2p)
	(8, 8)	Y	CCσ, CCπ, biradical (2 O2p), lone O2p → CCσ, COσ, biradical (far C2p, O2p), lone O2p
2	(12, 12)	N	4 CHσ, CCπ, biradical (2 O2p) → OHσ, 3 CHσ, CCπ, biradical (C2p, O2p)
3	(8, 8)	N	COσ, 2 CHσ, biradical (far C2p, O2p) → COσ, CHσ, COπ, biradical (far C2p; O2p, H)
	(10, 10)	Y	COσ, 2 CHσ, biradical(far C2p, O2p), lone O2p → COσ, CHσ, COπ, biradical (far C2p; O2p, H), lone O2p
4	(6, 6)	N	CCσ, COσ, biradical (far C2p, O2p) → COπ, COσ, biradical (far C2p, far C2p)
	(8, 8)	Y	CCσ, COσ, biradical (far C2p, O2p), lone O2p → COπ, COσ, biradical (far C2p, far C2p), lone O2p
5	(14, 14)	N	4 CHσ, CCσ, COσ, biradical (far C2p, O2p) → 4 CHσ, CCσ, COσ, biradical (near C2p, O2p)
6	(8, 8)	N	2 CHσ, COσ, biradical (far C2p, O2p) → COσ, CHσ, OHσ, biradical (2 C2p)
	(10, 10)	Y	2 CHσ, COσ, biradical (far C2p, O2p), lone O2p → COσ, CHσ, Ohσ, biradical (2 C2p), lone O2p
7	(8, 8)	Y	COσ, O2p, CCσ, biradical (near C2p; O2p, O2p) → COσ, 2 COπ, biradical (near C2p; O2p, far C2p)
8	(8, 8)	Y	COσ, O2p, CHσ, biradical (near C2p; O2p, O2p) → COσ, 2 COπ, biradical (near C2p; O2p, H)
9	(12, 12)	N	COσ, CCσ, 3 CHσ, biradical (near C2p, O2p) → COσ, CCσ, 2 CHσ, COπ, biradical (far C2p; O2p, H)
	(14, 13)	N	COσ, CCσ, 3 CHσ, biradical (near C2p, O2p), lone O2p → N/A
10	(12, 12)	N	2 CHσ, COσ, CCσ, CHσ, biradical (2 C2p) → 2 CHσ, COσ, CCσ, OHσ, biradical (near C2p, O2p)

[a] Only the lone pairs and bonding orbitals are shown; the antibonding orbitals can be inferred from bonding orbitals and the indication of in−out correlation. The O2s is always in the core.

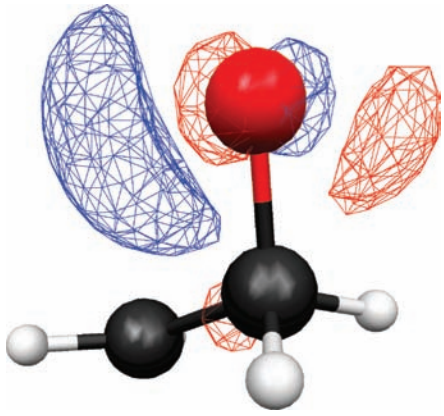

Figure 1. An example of an unphysical, in−out correlation, antibonding orbital found in active spaces that contain three O2p orbitals.

calculations larger than a (14, 14) active space are not feasible in GAMESS. Hence, this restriction limited the best active space for any reaction pathway. In choosing the CAS, the oxygen 2s (O2s) orbital was always placed in the core. Wherever possible, the oxygen 2p (O2p) orbital was included in the CAS; however, this inclusion quite often resulted in an unphysical, in−out correlation orbital (i.e., an additional mostly unoccupied orbital that resembles an O2p with an additional node, as shown in Figure 1). It is very important to understand the reasons for these choices. For this oxygen-containing system, the O2s orbital energy is significantly lower than that of the O2p energy. Hence, the O2s should usually not be important in the quasi-degenerate recovery of the correlation. As well, when the O2s was placed in the core or the active space, it remained doubly occupied and nondegenerate with orbitals required in the active space. Various attempts to place the O2s in the active space generally lead to additional difficulties in keeping an active space with consistent orbitals; these difficulties parallel the O2p-active space difficulties, which are discussed throughout the paper. Hence, placing both the O2s and O2p in the active space is both unnecessary and problematic.

In all of the reactions, a proper space without in−out correlation was not obtained after several, different, standard attempts. As an example, initial calculations constrained the orbital rotations so that the O2p remained a lone pair in the active space. However, when this constraint was released, the O2p flipped into the core, and a different bonding orbital moved from the core to the CAS. As well, other calculations initially placed the O2p in the core without constraints; these runs gave an "almost desired" active space with the O2p in the core and no in−out correlation in the active space. Then, increasing the space to include a lone O2p in the CAS and constraining the core orbital rotations caused an important antibonding orbital to move to the virtual space and an in−out correlation orbital to move to the CAS. Thus, various cases suggest in−out correlation leads to a lower-energy orbital root and makes its elimination from the active space difficult. As a result of these convergence issues, care is required to obtain smooth IRCs. For example, pathway 6 yielded a smooth IRC not only with in−out correlation and three O2p orbitals in the (10, 10) CAS but also without in−out correlation and two O2p orbitals in the (8, 8) CAS (e.g., one lone O2p orbital was placed in the MCSCF core). However, some cases required the three O2p orbitals and in−out correlation in the active space to obtain a smooth IRC. Furthermore, at some IRC points, the active space would require three antibonding orbitals if a CO π presented itself. Pathways 7 and 8 are examples of this situation, and in these cases, the inclusion of orbitals that look like a CO π*-bond automatically incorporated in−out correlation. In general, any other attempt for no in−out correlation and three O2p orbitals in the active space resulted in either orbital root changes

TABLE 2: barriers to Reactions in kcal/mol Calculated at the CASSCF Level without and with (in parentheses) ZPE[a]

reaction pathway	active space	CASSCF barrier 1[b]	CASSCF barrier 2[b]	Nguyen barrier 1[c]	Nguyen barrier 2[c]
1	(6, 6)	19.2 (19.3)	17.2 (16.4)	1.3	25.3
	(8, 8)	13.9 (14.3)	21.0 (20.5)		
2	(12, 12)	34.4 (30.3)	13.4 (12.0)	11.0	3.5
3	(8, 8)	18.7 (14.6)	14.9 (16.4)	15.3	8.3
	(10, 10)	15.1 (11.2)	17.1 (18.6)		
4	(6, 6)	18.1 (15.8)	17.7 (19.7)	22.1	4.7
	(8, 8)	13.9 (11.8)	19.3 (21.5)		
5	(14, 14)	48.3 (46.0)	51.5 (48.1)	31.5	39.9
6	(8, 8)	40.3 (37.6)	42.8 (39.8)	28.8	38.5
	(10, 10)	34.9 (32.4)	46.9 (43.8)		
7	(8, 8)	10.3 (8.0)	22.4 (26.5)	12.8	8.3
8	(8, 8)	16.3 (12.0)	20.1 (21.9)	17.4	8.5
9	(12, 12)	39.8 (34.4)	32.8 (34.0)	40.4	25.0
	(14, 13)	39.6 (34.1)	N/A		
10	(12, 12)	44.1 (40.7)	41.6 (39.1)	N/A	N/A

[a] Barrier 1 refers to the reactant−transition state barrier, and barrier 2 refers to the product−transition state barrier. [b] CASSCF barriers are obtained from unconstrained optimization of intermediates and ∼3−5 Å separated products. [c] Nguyen's barriers are the average barriers from different levels of theory listed in their publication.[5]

along the IRC or no existence of the desired root near a geometry that resembled the desired transition state.

Results and Discussion

Tables 2 and 3 give the overall barrier information for all reactions in the Introduction whereby each transition state divides each pathway into reactant/intermediate to transition state (barrier 1) and transition state to intermediate/product (barrier 2). Table 2 shows the CASSCF barriers with and without ZPE. Now, since both analytic gradients and Hessians at the MRMP2 level are unavailable in GAMESS, geometry optimizations, IRCs, and ZPEs at this level are not only numerically prohibitive but also can be numerically unfeasible for a single-state approach to quasi-degenerate, electronic states (in which the perturbation correction can be the most important). In particular, even in cases with symmetric stationary points, the MRMP2 Hessian requires asymmetric geometries where close-lying states then have no symmetry constraints. Since MR-AQCC ZPE are very similar to the CASSCF ZPE, ZPE are calculated only at the MCSCF level. However, single-point MRMP2 calculations were performed along the IRC (Table 3 shows the barriers). Although these barriers are not strictly barriers at the MRMP2 level, they should be representative of them. Single-point MRMP2 data at the MCSCF minima and maxima constitute stationary point MRMP2 (SPMRMP2) energy barriers, which always include ZPE. However, as will be shown, single-point MRMP2 energies along the IRC result in shifted barriers. These barriers are not true barriers at the MRMP2 level, but they strongly suggest that stationary points at the MRMP2 level do not always coincide with stationary points at the CASSCF level for a given CAS size. For cases when this shift is relatively large and that are critical to the dynamics (reactions 1, 3, and 4), MR-AQCC calculations are performed and discussed below. Table 4 gives the resultant MR-AQCC barriers as compared to CASSCF and shifted MRMP2 results.

In the rest of this section, specifics concerning each of the reactions are presented and discussed. In general, CAS size 1/CAS size 2 defines a CAS pair where the first CAS lacks in−out correlation and the second CAS has in−out correlation; except for the O2p and in−out correlation, the rest of the CAS pair active space is qualitatively the same. Here, comparisons of barriers include ZPE unless otherwise explicitly noted. All additional CAS studies (those not shown in Table 1) have only SPMRMP2, and the description will include those additional bonds that were added to the CAS beyond the standard CAS already given in Table 1. Examination of changes in bond length, natural orbital occupation numbers, and localized molecular orbital coefficients over the course of each reaction in different CAS sizes ultimately lead to the choice of the standard CAS.

Pathway 1:

$$\bullet\bullet O + C_2H_4 \rightarrow \bullet CH_2CH_2O\bullet$$

For pathway 1, the standard CAS pair is (6, 6)/(8, 8). This pathway has A″ symmetry only throughout barrier 1, which corresponds to the initial oxygen approach. The pathway becomes asymmetric along barrier 2 far from the transition state at the CASSCF level. As shown in Figure 2, the MRMP2 energy maximum does not coincide with the CASSCF energy maximum; performing single-point MRMP2 energies on the CASSCF IRC yields a small, horizontally shifted, MRMP2 energy maximum along the reaction coordinate. As well, this figure also reveals that the MRMP2 significantly changes the relative energetics, and hence, the CASSCF barrier 1 is substantially larger than that for MRMP2. Furthermore, as seen in Tables 2 and 3, neither CASSCF nor SPMRMP2 energies adequately describe barrier 1. Moreover, SPMRMP2 energies lead to a negative or neutral barrier in the initial addition of oxygen; this result emphasizes that pathway 1 energy barriers significantly shift with the addition of dynamic correlation. In fact, the reactant minimum also horizontally shifts.

Whereas the different active spaces give quite different CASSCF barriers, the shifted MRMP2 barriers are within 1 and 2 kcal/mol of each other for barriers 1 and 2, respectively. In addition, the CASSCF ZPE makes less than a 1 kcal/mol difference in the barriers. Taking into account both the transition state and the reactant shifts at the (8,8) CAS, barrier 1 changes to 1.9 kcal/mol (without ZPE, 2.3 kcal/mol with ZPE) and agrees quite well with the experimental, Arrhenius activation energy of 2.0 kcal/mol.[36,37] As well, Nguyen's average value of 1.3 kcal/mol for barrier 1 lies within 1 kcal/mol of the experimental activation energy.

To justify the size of the basis set selected, single-point CASSCF and MRMP2 energies were performed at the aug-cc-pVDZ and aug-cc-pVQZ levels at the aug-cc-pVTZ stationary points of this pathway. As well, CASSCF optimizations and

TABLE 3: Barriers to Reactions in kcal/mol Calculated at the MRMP2 Level[a]

reaction pathway	active space	MRMP2 barrier 1[b]	MRMP2 barrier 2[b]	Nguyen barrier 1[c]	Nguyen barrier 2[c]
1	(6, 6)	−1.5		1.3	25.3
		(2.4)	17.1		
		[2.5]	(21.9)		
		3.0[d]	[21.1]		
	(8, 8)	0.0			
		(1.4)	17.5		
		[1.8]	(19.8)		
		2.3[d]	[19.2]		
2	(12, 12)	8.9	4.4	11.0	3.5
		(13.4)	(6.4)		
		[9.3]	[4.9]		
		9.6[d]	5.3[d]		
3	(8, 8)	13.6	6.4	15.3	8.3
		(18.4)	(5.6)		
		[14.3]	[7.1]		
			7.4[d]		
	(10, 10)	14.0	5.0		
		(19.9)	(5.5)		
		[15.9]	[7.0]		
			7.3[d]		
4	(6, 6)	17.1	3.1	22.1	4.7
		(22.4)	(4.2)		
		[20.2]	[6.2]		
			5.8[d]		
	(8, 8)	16.9	1.8		
		(24.2)	(4.8)		
		[22.1]	[7.0]		
			6.8[d]		
5	(14, 14)	33.1	40.0	31.5	39.9
		(35.4)	(43.4)		
		[33.1]	[40.0]		
6	(8, 8)	25.7	34.1	28.8	38.5
		(28.4)	(37.2)		
		[25.7]	[34.1]		
	(10, 10)	26.7	35.6		
		(29.4)	(38.9)		
		[26.8]	[35.7]		
7	(8, 8)	8.9	6.5	12.8	8.3
		(15.2)	(6.4)		
		[12.9]	[10.6]		
			11.0[d]		
8	(8, 8)	16.4	5.7	17.4	8.5
		(24.4)	(7.6)		
		[20.1]	[9.4]		
			9.6[d]		
9	(12, 12)	39.1	24.7	40.4	25.0
		(45.0)	(24.0)		
		[39.6]	[25.2]		
	(14, 13)	37.1	N/A		
		(42.6)			
		[37.1]			
10	(12, 12)	27.6	28.4	N/A	N/A
		(31.0)	(31.0)		
		[27.6]	[28.4]		

[a] The bare number is the SPMRMP2 barrier (see text) and always includes CASSCF ZPE; the number in parentheses is the shifted barrier from the MRMP2 IRCs; and the number in square brackets is the shifted MRMP2 barrier, including ZPE from the MCSCF maxima and minima. Barrier 1 refers to the reactant-transition state barrier, and barrier 2 refers to the product-transition state barrier. [b] Single-point MRMP2 (SPMRMP2) values derive from CASSCF barriers, which are obtained from unconstrained optimization of intermediates and ∼3−5 Å separated products. [c] Nguyen's barriers are the average barriers from several different levels of theory that include ZPE listed in their publication.[5] [d] MRMP2 barrier with ZPE from shifts in minima in addition to shifts in transition states.

single-point MRMP2 energies were performed using the aug-cc-pVDZ basis. All calculations for the basis set validation used the (6,6) CAS for this pathway. In general, the optimized double-ζ results differed by 0.2 kcal/mol or less in comparison to the single-point double-ζ results at the aug-cc-pVTZ stationary points. For barrier 1 (barrier 2) with respect to the triple-ζ results, the double-ζ, single-point data differed by 0.7 (0.6) and 0.5 (1.1) kcal/mol for the CASSCF and SPMRMP2 data, respectively. For barrier 1 (barrier 2) with respect to the triple-ζ results, the quadruple-ζ, single-point data differed by 0.2 (0.2) and 0.1 (0.5) kcal/mol for the CASSCF and SPMRMP2 data, respectively. Thus, the triple-ζ results nicely approach the quadruple-ζ results even on a pathway where both vertical and horizontal shifting occur.

To justify the shifts in the barriers, optimizations for stationary points were carried out at the MRMP2 level. However, as

TABLE 4: MR-AQCC and Shifted MRMP2 Barriers (with shifted transition state only) in kcal/mol Given for Selected Reactions[a]

reaction pathway	active space	MRMP2 barrier 1	MRMP2 barrier 2	MR-AQCC barrier 1	MR-AQCC barrier 2
1	(6, 6)	(2.4)	(21.9)	4.2	19.4
	(8, 8)	(1.4)	(19.8)	3.5	22.1
				1.1	22.6
3	(8, 8)	(18.4)	(5.6)	18.4	8.8
	(10, 10)	(19.9)	(5.5)	17.9	8.9
				20.6	7.4
4	(6, 6)	(22.4)	(4.2)	22.4	6.7
	(8, 8)	(24.2)	(4.8)	24.2	6.2
				25.2	4.9

[a] The MR-AQCC results are shown with BS1, BS2, and BS3 from top to bottom in each grouping of the table. All barriers are reported without ZPE.

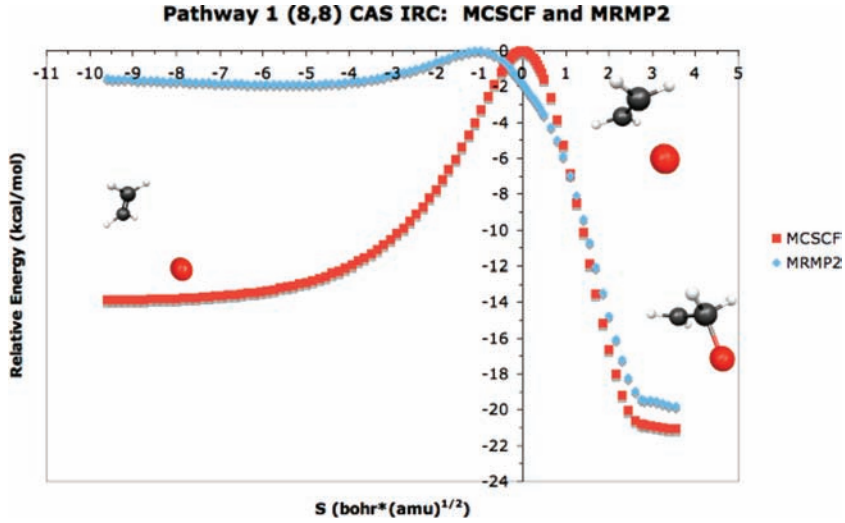

Figure 2. (8, 8) MCSCF and MRMP2 IRCs for pathway 1 display the shift in barriers. The plot below has the highest energies along the IRC for both levels of theory set equal.

already noted, a state-averaged CASSCF with quasi-degenerate perturbation approach is required here. As a result, slightly shifting the single state, MRMP2 values by the intruder state avoidance (ISA) technique led to pure state minima and a transition state of mixed symmetry for the (6, 6) CAS. The two resultant barriers from this ISA MRMP2 optimization match the best shifted barriers to within 1 kcal/mol. In particular, it is important to note that the shifted barriers are obtained using symmetry constraints; furthermore, ISA MRMP2 and shifted transition state geometries closely match. Thus, these shifted barriers are representative of the barriers at the MRMP2 level.

Since the MRMP2 recovery of dynamic correlation may or may not differ between different CAS sizes, we considered another CAS size for pathway 1: (14, 14) CAS with a core of O1s, two C1s, O2s, and lone O2p. This active space is comparable to the (6, 6) CAS with the addition of all the CH sigma bonds and antibonds to the active space. Barrier 1 for the (6, 6) and (14, 14) SPMRMP2 results without ZPE do not differ at all (i.e., 0.02 kcal/mol difference in the barrier 1). However, for the same CAS sizes, the (14, 14) SPMRMP2 without ZPE for barrier 2 gives a 1.9 kcal/mol higher barrier. Only small differences in the geometries of the two active spaces exist, and by performing (6, 6) single-point MRMP2 energies at the (14, 14) stationary points, ~1.5 kcal/mol results from changing the size of the active space.

Since this pathway is critical in the overall reaction and dynamic correlation plays a large role in its barriers, MR-AQCC calculations were performed (Table 4). The MRMP2 and MR-AQCC comparisons do not include ZPE since these are very similar for both levels of theory. Using the best basis set results for barrier 1, the shifted (8, 8) and (6, 6) MRMP2 result lies within 1 and 1.3 kcal/mol of the MR-AQCC result, respectively. For barrier 2, the shifted (6, 6) MRMP2 results lie within 1 kcal/mol of the MR-AQCC results, whereas the shifted (8, 8) now lies 2.8 kcal/mol below the MR-AQCC result. Since having all three O2p orbitals in the active space is important for barrier 1, the shifted (8, 8) MRMP2 results agree more with the MR-ACQQ. However, the agreement of the shifted (6, 6) with the MR-AQCC for barrier 2 suggests that in−out correlation may be numerically problematic at the MRMP2 level. It is interesting to note that the (14, 14) SPMRMP2 barrier matches the shifted (8, 8) MRMP2 barrier 2 at 19.8 kcal/mol, so very little is gained by increasing the CAS size.

The above effects of dynamic correlation give several differences in the geometry for the various assignments and levels of theory. The transition state CO σ is 2.05, 1.91, 1.99, 2.13, and 2.17 Å for Nguyen's B3LYP and this study's (6, 6) CAS, (8, 8) CAS, horizontally shifted (6, 6) CAS, and horizontally shifted (8, 8) CAS geometries, respectively. In addition, the barrier 2 intermediate OCCH dihedral angle freely rotates from 49 to 63° with an energy change of only 0.02 kcal/mol at the (6, 6) CASSCF level. The MR-AQCC and (8, 8) CAS geometries do not differ significantly with the exception that the barrier 2 intermediate has a dihedral angle of 41°.

For this pathway only, Nguyen et al. give constrained optimizations on the CO bond length at the CASSCF(8,8)/cc-pVDZ level with single-point CASPT2(8,8)/cc-pVDZ energies (CASPT2/CASSCF) for more accurate barriers in their study.

However, it is not clear what active space was used in this study. For barrier 2, Nguyen et al. calculated an average value of 25.3 kcal/mol, whereas constrained optimization energies at the CASPT2/CASSCF level gave ~22 kcal/mol, which closely agrees with the MR-AQCC result.

Pathway 2:

$$\bullet\bullet O + C_2H_4 \rightarrow \bullet OH + \bullet CH_2H_3$$

The entire reaction pathway has A″ symmetry unlike pathway 1. When oxygen abstracts a hydrogen from ethylene at a typical collisional energy in a CMBE, it encounters a large barrier 1. As with the case of pathway 1 and many of the other barriers present here, dynamic correlation significantly lowers the barriers for the reaction at the (12, 12) CASSCF stationary points (from 30.3 to 8.9 kcal/mol for barrier 1 and from 12.0 to 4.4 kcal/mol for barrier 2 from CASSCF to SPMRMP2 values). As a general trend, MRMP2 always energetically lowers CASSCF barriers by a much more substantial amount in the cases of bimolecular products to transition state barriers than in the cases of unimolecular intermediate to transition state barriers.

However, for this case, dynamic correlation gives no significant differences in the geometries since the barriers do not horizontally shift by much. The energy change between the SPMRMP2 barriers and the shifted barriers is small (less than 1 kcal/mol) with or without shifts in the minima. However, the geometric changes due to the transition state horizontal shift along the IRC remain small in the (12, 12) CAS in comparison to the minima horizontal shifts. CASSCF ZPE changes barrier 1 by 4.1 kcal/mol—a significant change—and barrier 2 by 1.5 kcal/mol. For the shifted MRMP2 barriers, barrier 1 lies 1.4 kcal/mol below Nguyen's average barrier 1, and barrier 2 lies 1.8 kcal/mol above Nguyen's average barrier 2. However, the products in our work have a potential well when the OH is ~3 Å from the closest carbon. At the 50 Å distance, barrier 2 is smaller by ~1.4 kcal/mol on the basis of the SPMRMP2 value at the ~3 Å distance. SPMRMP2 barrier 1 at 50 Å is 0.3 kcal/mol smaller than SPMRMP2 barrier 1 from the ~3 Å minimum.

CASSCF runs could not produce a (14, 14) CAS with in−out correlation for this pathway; the O2p orbital tended to flip from the CAS to the core toward the reactant end of the IRC. We also investigated (8, 8) and (10, 10) CASs, in which all nonaction CH σ's (i.e., those not directly involved in the hydrogen abstraction) from the standard (12, 12) CAS were placed in the core and the CC σ was placed in the active space for the (10, 10). Both these CASs have in−out correlation. The (8, 8) and (10, 10) CASs have all SPMRMP2 barriers within 1 kcal/mol of each other; however, these nondegenerate, in−out correlation barriers differ from the (12, 12) CAS barriers without in−out correlation by ~1 and ~2.4 kcal/mol for barriers 1 and 2, respectively. The barriers calculated from the (12, 12) CAS represent the overall process better.

Pathway 3:

$$\bullet CH_2CH_2O\bullet \rightarrow \bullet CH_2CHO + \bullet H$$

The standard CAS pair for pathway 3 is (8, 8)/(10, 10). As with the rest of the pathways on the lowest-lying triplet surface in this paper, pathway 3 is asymmetric. Including the dynamic correlation here gives a large horizontal shift in the transition state but no significant horizontal shift for the products of barrier 2. However, the shift in the transition state does change the geometries, and hence barrier energies change as well. Between the various levels of theory and shifted geometries, the dissociating H−C distance in the transition state (the action CH σ) is 1.77, 1.62, 1.57, 1.74, and 1.57 Å for Nguyen's B3LYP and this study's (8,8) CAS, (10,10) CAS, horizontally shifted (8,8) CAS, and horizontally shifted (10,10) CAS geometries, respectively. For the MRMP2 barriers with a shifted transition state with respect to the SPMRMP2 barriers, barriers 1 and 2 both increase by only 0.7 kcal/mol in the (8,8) CAS while both barriers 1 and 2 increase by 1.9−2.0 kcal/mol in the (10,10) CAS. Again, minima shifts do not make much difference in this analysis. Furthermore, the shifted (8,8) and (10,10) MRMP2 barrier 2s are almost identical while the shifted (10,10) MRMP2 barrier 1 lies 1.6 kcal/mol above the corresponding shifted (8,8) value. CASSCF ZPE lowers barrier 1 by ~4.0 kcal/mol (again, a rather significant effect) and raises barrier 2 by 1−2 kcal/mol. Now, both the shifted (8,8) and (10,10) MRMP2 barrier values lie within 1 kcal/mol of Nguyen's average barriers. All of the shifted MRMP2 barriers are within 2 kcal/mol of the MR-AQCC/BS3 results with the (10,10) within 1 kcal/mol for barrier 1.

For this pathway, including the CC σ in the active space has a small effect since the CC σ length changes by only 0.05 Å. For the SPMRMP2 barriers, incorporating the CC σ into larger (10,10) and (12,12) CAS calculations leads to a ~1 kcal/mol and ~0.5 kcal/mol change from the (8,8) and (10,10) barriers 1 and 2, respectively.

Pathway 4:

$$\bullet CH_2CH_2O\bullet \rightarrow \bullet\bullet CH_2 + H_2CO$$

The (6,6)/(8,8) CAS pair describes how the main biradical intermediate splits into biradical methylene and formaldehyde. For this reaction, dynamic correlation shifts both the transition state and the barrier 2 minimum. Such shifts substantially alter both the reaction coordinate and the energy of the transition state but do not significantly change the barrier 2 minimum energy. As a result, the various levels of theory give differences in the geometries. For the transition state, the action CC σ is 2.28, 2.00, 1.94, 2.23, and 2.21 Å for Nguyen's B3LYP and this study's (6, 6) CAS, (8, 8) CAS, horizontally shifted (6, 6) CAS, and horizontally shifted (8, 8) CAS geometries, respectively. In addition, barrier 2 bimolecular intermediate (approaching products) has (6, 6) CAS, (8, 8) CAS, horizontally shifted (6, 6) CAS, and horizontally shifted (8, 8) CAS geometries with CC distance of 4.14, 4.16, 3.40, and 3.50 Å, respectively. This distance results from a hydrogen bonding potential well from the bimolecular intermediate, which approaches the products at larger distances. These geometrical differences result in various energy changes. For the MRMP2 barriers with a shifted transition state with respect to the SPMRMP2 barriers, both barriers 1 and 2 increase by 3.1 and 5.2 kcal/mol in the (6, 6) and (8, 8) CAS, respectively. Once again, including the minima shift does not make much difference to these observations, so even though a significant geometrical change occurs, very little difference in the energetics results. The shifted (8, 8) and (10, 10) MRMP2 barriers lie within 1 kcal/mol of each other for barrier 2, whereas for barrier 1, the shifted (10, 10) value lies 1.9 kcal/mol above the corresponding (8, 8) value. For barrier 1, the SPMRMP2 (6, 6) and (8, 8) barriers lie within 1 kcal/mol, whereas the SPMRMP2 (8, 8) barrier 2 lies 1.3 kcal/mol above the corresponding (6, 6) barrier 2. The MR-AQCC calculations show agreement with the shifted MRMP2 to within 1 kcal/mol for the (8, 8) active space. CASSCF ZPE changes

all barriers by ~2.2 kcal/mol, so in comparison to Nguyen's values, the (6, 6) MRMP2 barrier 1 lies 1.9 kcal/mol below the average barrier 1, and the (8, 8) MRMP2 barrier 1 matches Nguyen's average barrier 1. For the MRMP2 barrier 2, the (6, 6) CAS lies 1.5 kcal/mol above, and the (8, 8) CAS lies 2.3 kcal/mol above Nguyen's average.

Larger (10, 10) and (12, 12) CAS that include additional correlation from the formaldehyde two CH σ's were investigated. Here, barrier 2 values are within 1 kcal/mol; however, barrier 1 values are ~2−3 kcal/mol higher. However, the values compared are SPMRMP2 values, and the shift will be different for different CAS sizes. It should be noted that unlike in pathway 1, the CH σ's on different carbons are never degenerate; however, not including some quasi-degenerate CH σ's in the active space might lead to undesirable results, as well.

Pathway 5:

$$\bullet CH_2CH_2O\bullet \rightarrow \bullet CH_3 + CHO\bullet$$

In this pathway, a hydrogen shifts from one carbon to the other carbon. As a result of the large (14, 14) CAS size, dynamical correlation did not lead to any reportable geometry shifts. In addition, the (14, 14) CAS geometry does not differ from Nguyen's B3LYP in any significant way. In addition, as a result of the large CAS size, the MRMP2 barriers do not exhibit any difference from the SPMRMP2 barriers. No comparison for in−out correlation exists here for various reasons (see below). The CASSCF ZPE give a substantial change of 2.3 kcal/mol for barrier 1 and 3.4 kcal/mol for barrier 2. The MRMP2 barrier 1 lies 1.6 kcal/mol above Nguyen's average barrier 1, and the MRMP2 barrier 2 lies within 1 kcal/mol of Nguyen's barrier 2.

This hydrogen shift between the two carbons could be explored only without in−out correlation; any attempt to find a transition state with in−out correlation in a smaller CAS where the active space does not include degenerate hydrogens failed. Here, in−out correlation orbitals do not lead to a qualitatively correct, ground-state wave function. In addition, the (14, 14) CAS includes the CO σ in the active space; an attempt to include the O2s, CO σ, and O2p in the core in a (12, 12) CAS leads to mixing of the O2s and CO σ. Oftentimes, such a mixing, or polarization, of the O2s leads to improper orbital root changes later on in the IRC. As well, the active space also requires inclusion of the CC σ since this bond is mixed with the shifting hydrogen. Hence, these issues lead to the choice of active space.

SPMRMP2 barriers for an (8,8) CAS with a core of O2s, all nonaction CH σ's, and O2p, (12, 12) CAS with a core of O2s, CO σ, and O2p, and (12, 12) CAS with a core of O2s, CH σ nearest the oxygen, and O2p were also found. Barrier 1 values are all within ~1 kcal/mol of each other; however, barrier 2 values differ by the active space chosen and range from 37.9 to 41.7 kcal/mol. In particular, the (12, 12) barriers with the quasi-degenerate hydrogen in the core lie within 1 kcal/mol of the (14, 14) barriers.

Pathway 6:

$$\bullet CH_2CH_2O\bullet \rightarrow \bullet CH_2 + CHOH$$

In this reaction, the hydrogen shifts from carbon to oxygen and requires a (8, 8)/(10, 10) CAS pair. The core includes the CC σ, which changes by only 0.02 Å over the entire reaction. Here, dynamic correlation does not horizontally shift any of the CASSCF stationary points by a significant amount. However, the barrier 2 intermediate has two conformers with no geometrical differences in addition to a hydroxyl rotation. The lowest-energy conformer has a HCOH dihedral of 179° (trans-like); the higher-energy conformer has a corresponding 36° dihedral angle (cis-like); both conformers have COH angles of 108° with an energy difference of 0.2−0.3 kcal/mol at the CASSCF level. For the shifted MRMP2 barriers with respect to the SPMRMP2 barriers, all barriers change by, at most, 0.1 kcal/mol. The shifted (10, 10) MRMP2 barrier 1 lies 1.1 kcal/mol above the corresponding shifted (8, 8) barrier 1, and for barrier 2, the shifted (10, 10) barrier lies 1.6 kcal/mol above the corresponding (8, 8) value. CASSCF ZPE significantly changes barrier 1 by ~2.7 kcal/mol and barrier 2 by ~3.1 kcal/mol both with and without in−out correlation. For the shifted (10, 10) MRMP2 barriers, barrier 1 lies 2.0 kcal/mol lower than Nguyen's average barrier 1, and barrier 2 lies 2.8 kcal/mol below Nguyen's average barrier 2. The smaller (8, 8) comparisons to Nguyen's barriers give barrier 1 lower by 1.1 kcal/mol and barrier 2 lower by 1.6 kcal/mol.

Pathway 7:

$$CH_3\bullet CHO\bullet \rightarrow \bullet CH_3 + \bullet CHO$$

This dissociation involves all CO π bonds and must contain in−out correlation to obtain a CASSCF solution with the FULLNR converger. For this pathway, dynamic correlation leads to a large horizontal shift in both the transition state and barrier 2 products. MR-AQCC calculations were not performed here since the previous results show the error at the MRMP2 level is at worst, 3 kcal/mol and most likely less. Geometrical differences include the transition state CC σ of 2.12, 1.89, and 2.12 Å for Nguyen's B3LYP, (8, 8) CAS, and shifted (8, 8) CAS geometries, respectively. In addition, barrier 2 products have CC σ's of 4.09 and 3.40 Å for the CAS and shifted CAS geometries, respectively. For the shift in the barriers from the transition state shift as compared to SPMRMP2 barriers, barriers 1 and 2 increase by ~4 kcal/mol for the shifted barriers, a large effect. As for the effect of the barrier 2 minimum geometry shift on the energies, this shift increases the overall barrier 2 by 0.4 kcal/mol. CASSCF ZPE decreases barrier 1 by 2.3 kcal/mol and increases barrier 2 by 4.2 kcal/mol. For the shifted MRMP2 barriers, barrier 1 agrees with Nguyen's barrier 1, and barrier 2 is 2.3 kcal/mol higher than the Nguyen values.

A (10, 10) CAS with additional correlation from the CH σ nearest the oxygen gives SPMRMP2 barriers within 1 kcal/mol of the corresponding (8, 8) barriers. Any attempt to exclude in−out correlation via a core, lone O2p orbital leads to unwieldy iterations toward the dissociation end of the IRC; these large iterations indicate inappropriate orbital root changes.

Pathway 8:

$$CH_3\bullet CHO\bullet \rightarrow \bullet CH_3\bullet CO + \bullet H$$

This dissociation also involves all CO π bonds and must contain in−out correlation to converge with the FULLNR converger to a CASSCF solution; hence, it requires an analysis almost identical to that of pathway 7. Both the transition state and barrier 2 products exhibit large horizontal shifts in the IRC with MRMP2. As for the resulting geometry changes, the transition state action CH distance is 1.78, 1.51, and 1.72 Å for Nguyen's B3LYP, (8, 8) CAS, and shifted (8, 8) CAS geometries, respectively. As with pathway 7, the B3LYP results agree with the shifted CAS geometries in the transition state.

In addition, the barrier 2 product action CH σ is 5.35 and 3.58 Å for CAS and shifted CAS geometries, respectively. There is a dramatic change between the transition state, shifted MRMP2 barriers and the SPMRMP2 barriers; both barriers 1 and 2 shift by 3.7 kcal/mol. As for the effect of the barrier 2 minimum geometry shift on the energies, this shift increases the overall barrier 2 by 0.4 kcal/mol. CASSCF ZPE increases barrier 1 by 4.3 kcal/mol and barrier 2 by 1.8 kcal/mol. For the shifted MRMP2 barriers, barrier 1 lies 2.7 kcal/mol above Nguyen's average barrier 1, and barrier 2 lies about 1 kcal/mol higher than Nguyen's average barrier 2.

A (10, 10) CAS with additional correlation from the CC σ gives SPMRMP2 barriers within 1 kcal/mol of the corresponding (8, 8) barriers. Again, any attempt to exclude in−out correlation via a core, lone O2p orbital leads to unwieldy iterations toward the dissociation end of the IRC.

Pathway 9:

$$CH_3\bullet CHO\bullet \rightarrow \bullet H + \bullet CH_2CHO$$

In this pathway, hydrogen dissociates and actually requires three O2p orbitals in the active space for the possibility of a smooth IRC. The (12, 12) CAS, which does not include all three O2p orbitals, does not have a smooth IRC because a discontinuity appears a few steps toward the barrier 2 product where a lone, core O2p violently changes orientation. Likewise, the biradical, active space O2p violently changes orientation at the same IRC point. Thus, the active space must contain all three O2p orbitals to produce a smooth IRC. However, for this pathway in a (14, 14) CAS, having three active space O2p orbitals and in−out correlation does not lead to a transition state. Thus, in a fashion similar to the in−out correlation problem in pathway 5, the (14, 14) CAS here does not lead to a wave function, which is qualitatively consistent with smaller CAS wave functions that lack in−out correlation. However, a (14, 13) CAS with no in−out correlation leads to an IRC that consistently maintains its active space toward the barrier 1 intermediate. However, the first IRC step toward the products leads to unwieldy energy iterations and eventually to too many constrained optimizations in the IRC itself. The unwieldy iterations occur because the converger leads to orbital rotations that try to incorporate in−out correlation as the reaction moves toward the products. In other reaction pathways that include in−out correlation (when possible) from the start, the in−out correlation tends to become or make up the CO π^*. However, with a (14, 13) CAS, this reaction pathway starts with no in−out correlation at the transition state and then subsequently develops in−out correlation in a linear combination with the CH σ^* and displaces the CC σ^* during the geometry changes, so we do not report (14, 13) results for barrier 2.

For this pathway, neither the large (12, 12) or the (14, 13) CAS have much of a horizontal shift in the IRC from dynamic correlation. The minima do not horizontally shift at all from the MRMP2. No noteworthy geometry differences occurred between this study and Nguyen's results. For the SPMRMP2 barriers with respect to the shifted barriers, the (12, 12) barriers shift by less than 1 kcal/mol, and the (14, 13) barrier 1 does not shift at all. CASSCF ZPE lowers barrier 1 by ~5.5 kcal/mol and increases barrier 2 by ~1.2 kcal/mol. For the shifted MRMP2 barriers, both (12, 12) CAS barrier 1 and 2 correspondingly lie within 1 kcal/mol of Nguyen's values. With the additional O2p in the active space (14, 13), barrier 1 decreases by 2.5 kcal/mol.

Pathway 10:

$$CH_3\bullet CHO\bullet \rightarrow \bullet CH_2\bullet CHOH$$

This hydrogen shift requires at minimum a (12, 12) CAS. This large CAS size leads to no horizontal shifts. As before with the other CAS sizes, no substantial geometry differences exist in the minima, although the dynamic correlation does change the overall barriers. Since Nguyen et al. do not solve for this transition state, no comparisons can be made in this respect. As well, from previous data and the necessary CAS size, the (12, 12) should provide an adequate solution for this particular reaction. The CASSCF ZPE decreases barrier 1 by 3.4 kcal/mol and increases barrier 2 by 2.5 kcal/mol.

Surface Crossings: Preliminary Investigation at the MCSCF Level. Several factors come into play in the location of relevant, close-lying electronic states. First and foremost, active space choice affects the electronic states found; a reasonable active space will lead to the states of interest. Second, the character (i.e., the spatial and spin characteristics) of an initial guess relative to the desired molecular orbitals along with the number of CI roots requested determines the kinds of states located; a good guess at the initial molecular orbitals along with a reasonable number of CI roots will minimize the number of missed electronic states. Determining a reasonable number of states to request requires some experimentation; the lowest-lying energies from calculations with different numbers of CI roots can always be compared. In this discussion, a resultant electronic state with an exact density refers to any state of interest obtained by optimizing a particular set of orbitals and CI coefficients under given spin and spatial (if any) symmetries.

On the basis of the above description, CI energy runs with several roots and with both singlet and triplet multiplicities were performed on all the lowest-lying triplet stationary points to estimate the relative location of nearby states. In addition, separate energy calculations of the A′ surface were run for pathways 1 and 2 to account for higher symmetry states. While certainly not quantitative, these calculations provide a preliminary analysis on the locations of surface crossings, which will be explored in more detail in future work. For this analysis, we report any states near the lowest-lying triplet within ~10 kcal/mol and also note any singlet states below the lowest-lying triplet. In the analysis below, ground state means the lowest state of either the triplet or singlet states. In addition, energetics for the lowest singlet and triplet are always determined from the exact densities. For any close-lying, higher, inexact roots, we note which exact density (singlet or triplet along with spatial symmetry if any) yields, or derives, the higher root of interest. Furthermore, any barriers reported are SPMRMP2 barriers.

For pathway 1, the transition state and barrier 2 intermediate have close-lying states. For the transition state, neither the (6, 6) nor the (8, 8) CAS can adequately describe the triplet A′ with an exact density (i.e., orbital root flipping occurs), so a (4, 4) CAS A′ energy on the triplet (4, 4) CAS A″ transition state and a (4, 4) CAS A′ transition state were found; this (4, 4) CAS contains only the biradical and CO σ/CC π. These calculations show an A′−A″ energy difference of only 0.6 kcal/mol, and the A′ transition state also lies 0.6 kcal/mol above the triplet A″ stationary state. These results lie within 1 kcal/mol of other calculations in the literature.[5,11] The barrier 2 intermediate has a triplet state above its singlet ground state by 0.6 and 1.3 kcal/mol for the (6, 6) and (8, 8) CAS, respectively. In addition, another singlet state derived from the triplet density lies 2.6 kcal/mol above the triplet in both the (6, 6) and (8, 8) CAS.

For pathway 2, as the products are separating and each going to doublet states, the overall singlet and triplet surfaces for the reactions become degenerate. It is interesting to note that Nguyen et al. found a triplet A′ state less than 1 kcal/mol above the triplet A″ ground state; however, the (12, 12) CAS did not give this result. It gives the triplet A′ state as ∼70 kcal/mol above the lowest-lying triplet A″ state with exact densities. However, the previously mentioned (14, 14) CAS with root flipping gives a triplet A′ state ∼10 kcal/mol above the triplet A″ ground state.

Furthermore, SPMRMP2 on this triplet A″ stationary point yields the triplet A′ as lying ∼0.5 kcal/mol below the triplet A″ state. Although the order of states interchanges with the application of MRMP2, a quasi-degenerate perturbation calculation should give the same ordering as the CASSCF results. However, such a calculation is currently prohibitive in GAMESS in the configuration state function code. This particular example shows the importance of selecting the active space to yield the desired electronic states.

For pathway 3, the barrier 1 minimum has a singlet state 1.5 kcal/mol above the triplet ground state for both the (8, 8) and (10, 10) CAS. This minimum corresponds to the barrier 2 minimum in pathway 1. Examination of the two structures shows that the IRCs for different pathways lead to different conformers, which interchange state orders near the regions of the ISC. This behavior results from the free OCCH dihedral angle (as discussed above in pathway 1) and shows this particular biradical definitely has a surface crossing and possibly several surface crossings at that. In addition to these results, the transition state has a singlet that exists above the triplet ground state by 7.4 and 3.4 kcal/mol for the (8, 8) and (10, 10) CAS, respectively. SPMRMP2 corrections to these energy differences in the singlet versus the ground state triplet lead to 5.2 and 3.9 kcal/mol for the (8, 8) and (10, 10) CAS, respectively. As for barrier 2, the IRC leads to a doublet whereby the singlet and triplet energies become degenerate for both the (8, 8) and (10, 10) CAS.

Barrier 1 in pathway 4 corresponds to the predominant triplet−singlet surface crossing biradical already mentioned several times; this biradical will not be mentioned again since the same results hold for all CAS sizes. On the basis of this analysis, this pathway contains no other close-lying states, and the lowest-lying triplet state appears to remain the ground state through the rest of the pathway.

In pathway 5, barrier 2 intermediate has a singlet ground state that lies 60.6 kcal/mol below the lowest-lying triplet state. Furthermore, a second excited singlet state derived from the triplet density lies ∼3.6 kcal/mol above the lowest-lying triplet state. As a result, the transition state geometry also has a singlet ground state with a triplet that lies 50.9 kcal/mol above it. The second excited state singlet was not found from the triplet state density, suggesting that the ground state singlet density better describes the singlet excited state.

The transition state for pathway 6 has a singlet above the ground state triplet by 0.4−0.5 kcal/mol for the (10, 10) and (8, 8) CAS. The second excited state triplet provided by the singlet density lies 0.4−0.6 kcal/mol above the first excited state singlet for the (8, 8)/(10, 10) CAS pair. This pathway's barrier 2 intermediate has a triplet ground state with a singlet that lies 1.7 kcal/mol above it for the (8, 8)/(10, 10) CAS pair.

Pathway 7 has a singlet ground state throughout. Now the barrier 1 intermediate is identical to the barrier 2 in pathway 5 and, thus, has the lowest-lying triplet far above the singlet ground state again. This result for this intermediate also occurs in pathways 8 and 9. The lowest-lying triplet for the transition state lies 46.4 and 44.7 kcal/mol above the ground state singlet for the (8, 8) and (10, 10) CAS, respectively. The barrier 2 products in pathway 7 dissociate to doublets; this dissociation results in overall degenerate singlet and triplet surfaces.

Both pathways 8 and 9 have a singlet ground state throughout the whole path. Pathway 8 calculations do not reveal any close-lying states for the triplet of interest. As for pathway 9, it has the intermediate common to pathways 5, 7, and 8. However, the (12, 12) and (14, 13) CAS also give a second excited state singlet derived from the triplet density above the lowest triplet by 4.0 and 5.8 kcal/mol, respectively. Pathway 5 has the same state ordering. Barrier 2 minimum analysis is given in reaction pathway 3.

For the additional reaction pathway 10 located in this paper, intermediates have already been analyzed in earlier pathways 5−9. However, analysis of the transition state shows the lowest-lying triplet lies 15.0 kcal/mol above the ground state singlet. As well, a second excited singlet state derived from the triplet density again lies within a few kilocalories per mole of the lowest triplet state.

Conclusions

In the current study, CASSCF and MRMP2 provide accurate barriers and minimum energy paths for the lowest-lying triplet of O + ethylene, and additional single-point calculations with more states for the singlet and triplet at the triplet geometries yield preliminary surface crossing data. MR-AQCC calculations to examine additional correlation effect for reactions 1, 3, and 4 usually give differences from the MRMP2 values of less than 1 kcal/mol. Some exceptions are the difference of ∼2 kcal/mol for reaction 3 barrier 2 and ∼3 kcal/mol for barrier 1 in reaction 1. As noted earlier, the near low-lying states that are likely causing these larger differences will require other approaches, such as state-averaged wave functions, and will be examined in future work. Figure 3 summarizes the energetics of the lowest triplet surface with the best MRMP2 values from this work. During the course of the investigation, the act of choosing an active space reveals several issues within the framework of this study. For several of the reaction pathways, root flipping shows that the converger cannot provide the most proper active space for a particular CAS size that would recover the majority of the static correlation. As a result, CASs with and without in−out correlation are constructed, and various issues and differences arise from this compromise at both the CASSCF and MRMP2 levels. However, these issues appear to be minor with respect to the energetics. As already discussed in particular, the existence of certain CASSCF stationary points gets called into question when these extrema exist only without in−out correlation; as such, the CAS constructions with in−out correlation can be considered improper for those particular reactions.

As well, MRMP2 energies on top of various CASs lead to several items of note. First, as evident from the single-point MRMP2 runs, obtaining reasonable energetics for the barriers requires the inclusion of dynamic correlation in some fashion. In this study, correlation from MRMP2 lowers energy barriers in many but not all cases, and in most cases, MRMP2 single-point energies along the IRC tend to shift the location of energy maxima and minima and, hence, change the overall barrier. In particular, (12, 12) and larger CASs do not experience much of a horizontal, or geometrical, shift but

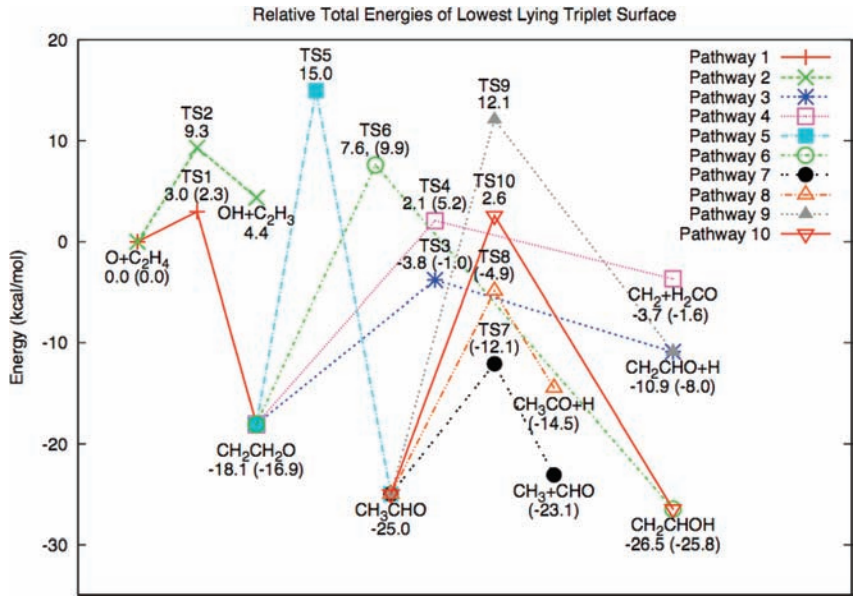

Figure 3. Total MRMP2 energies relative to reactants O + C_2H_4 for the overall lowest-lying triplet surface. All relative energies are constructed in a piece-wise fashion to give an energy relative to the initial reactants. Values in parentheses derive from a CAS with in−out correlation, and plain values derive from a CAS with no in−out correlation.

still experience a vertical, or energy, shift that drastically changes the barrier. A smaller CAS may or may not experience a geometrical shift with the addition of dynamic correlation. Second, the various CASs lead to similar but not identical barriers that lie within ∼1−2 kcal/mol. Third, MRMP2 corrections affect the energetics more in the cases of bimolecular products to transition state barriers than in the cases of unimolecular intermediate to transition state barriers.

As a result of the above multireference outcomes, the lowest-lying triplet barriers in this study qualitatively agree with Nguyen's barriers. However, not all barriers lie within chemical accuracy of one another. Certain barriers differ for distinct physical reasons other than the inclusion of correlation. For example, both barriers in pathway 2 and barrier 2 in pathway 4 in this study account for hydrogen bonding; hence, a substantial difference in barriers occurs between the two studies. On the other hand, evidence suggests the dynamic correlation energetically alters barrier 2 in pathway 1 and both barriers in pathway 6. As well, both barrier 2 in pathway 7 and barrier 1 in pathway 8 differ by 2.7 kcal/mol from Nguyen's corresponding barriers. In addition to these comparisons, barrier 1 in pathway 9 provides some insight into the energetic difference between a proper active space and a single, compromised active space. In the final path 10, the hydrogen shift from the far carbon to the oxygen was found.

The preliminary surface crossing analysis confirms the predominant surface crossing(s) for the system to be around the CH_2CH_2O biradical. However, several more crossings become important with hyperthermal considerations. The first and second excited states for the CH_3CHO biradical lie close to one another. As well, in the pathway 3 dissociation, a singlet state lies within ∼5 kcal/mol of the lowest-lying triplet transition state. The entire reaction pathway 6 has close-lying triplet and singlet states, and the transition state itself has an additional close-lying second excited state singlet. This nearby state at least partially explains why the results from pathway 6 significantly differ from others' results. This study also shows that some excited state characterizations require the inclusion of the O2p in the active space (e.g., pathway 2).

Future research will involve a close examination of the singlet surface, the location of the surface crossing using state averaged MCSCF, and the spin−orbit coupling near these crossings. These results will be used to fit to semiempirical methods, such as those of Granucci and Toniolo,[38] and then perform dynamics.

Acknowledgment. The authors are indebted to Michael W. Schmidt and Mark S. Gordon for help in using the capabilities of GAMESS and MCSCF. This material is based upon work supported by the National Science Foundation under Grant no. OISE-0730114 for the Partnerships in International Research and Education (PIRE) and by the Robert A. Welch Foundation under Grant no. D-0005. TeraGrid resources were provided by the Texas Advanced Computing Center (TACC). Support was also provided by the High-Performance Computing Center (HPCC) at Texas Tech University, under the direction of Philip W. Smith. In addition, this work was supported by the Austrian Science Fund within the framework of the Special Research Program F16 (Advanced Light Sources) and Project P18411-N19. T.L.W. acknowledges computing resources purchased through funds provided by Ames Laboratory and Iowa State University.

Supporting Information Available: Additional information including the CASSCF and relevant MR-AQCC geometries, absolute energies, frequencies, ZPE, and moments of inertia along with absolute MRMP2 energies. This material is available free of charge via the Internet at http://pubs.acs.org.

References and Notes

(1) Gardiner, W. C., Jr., Ed.; *Combustion Chemistry*; Springer-Verlag: New York, 1984.

(2) Casavecchia, P.; Capozza, G.; Segoloni, E.; Leonori, F.; Balucani, N.; Volpi Gian, G. *J. Phys. Chem. A* **2005**, *109*, 3527.

(3) Su, H.; Zhao, S.; Liu, K.; Xiang, T. *J. Phys. Chem. A* **2007**, *111*, 9600.

(4) Lee, S.-H.; Huang, W.-J.; Chen, W.-K. *Chem. Phys. Lett.* **2007**, *446*, 276.

(5) Nguyen, T. L.; Vereecken, L.; Hou, X. J.; Nguyen, M. T.; Peeters, J. *J. Phys. Chem. A* **2005**, *109*, 7489.

(6) Yamaguchi, K.; Yabushita, S.; Fueno, T.; Kato, S.; Morokuma, K. *Chem. Phys. Lett.* **1980**, *70*, 27.
(7) Dupuis, M.; Wendoloski, J. J.; Takada, T.; Lester, W. A., Jr. *J. Chem. Phys.* **1982**, *76*, 481.
(8) Fueno, T.; Takahara, Y.; Yamaguchi, K. *Chem. Phys. Lett.* **1990**, *167*, 291.
(9) Jursic, B. S. *THEOCHEM* **1999**, *492*, 85.
(10) Smith, B. J.; Nguyen Minh, T.; Bouma, W. J.; Radom, L. *J. Am. Chem. Soc.* **1991**, *113*, 6452.
(11) Hu, W.; Lendvay, G.; Maiti, B.; Schatz, G. C. *J. Phys. Chem. A* **2008**, *112*, 2093.
(12) Curtiss, L. A.; Raghavachari, K.; Redfern, P. C.; Rassolov, V.; Pople, J. A. *J. Chem. Phys.* **1998**, *109*, 7764.
(13) Montgomery, J. A., Jr.; Frisch, M. J.; Ochterski, J. W.; Petersson, G. A. *J. Chem. Phys.* **1999**, *110*, 2822.
(14) Mebel, A. M.; Morokuma, K.; Lin, M. C. *J. Chem. Phys.* **1995**, *103*, 7414.
(15) Werner, H. J.; Knowles, P. J. *J. Chem. Phys.* **1988**, *89*, 5803.
(16) Knowles, P. J.; Werner, H. J. *Chem. Phys. Lett.* **1988**, *145*, 514.
(17) Gordon, M. S.; Schmidt, M. W. *Theory Appl. Comput. Chem.: First Forty Years* **2005**, 1167.
(18) Roos, B. *Adv. Chem. Phys.* **1987**, *69*, 399.
(19) Ruedenberg, K.; Sundberg, K. R. *Quantum Sci.* **1976**, 505.
(20) Schmidt, M. W.; Gordon, M. S. *Annu. Rev. Phys. Chem.* **1998**, *49*, 233.
(21) Dunning, T. H., Jr. *J. Chem. Phys.* **1989**, *90*, 1007.
(22) Ivanic, J.; Ruedenberg, K. *Theor. Chem. Acc.* **2001**, *106*, 339.
(23) Lengsfield, B. H., III. *J. Chem. Phys.* **1980**, *73*, 382.
(24) Dupuis, M.; Mougenot, P.; Watts, J. D. In *Modern Techniques in Theoretical Chemistry*; Clementi, E., Ed.; ESCOM: Leiden, 1989.
(25) Yarkony, D. R. *Chem. Phys. Lett.* **1981**, *77*, 634.
(26) Bauschlicher, C. W., Jr. *J. Chem. Phys.* **1980**, *72*, 880.
(27) Boys, S. F. *Quantum Theory At., Mol., Solid State.* **1966**, 253.
(28) Gonzalez, C.; Schlegel, H. B. *J. Chem. Phys.* **1989**, *90*, 2154.
(29) Hirao, K. *Chem. Phys. Lett.* **1992**, *190*, 374.
(30) Nakano, H. *J. Chem. Phys.* **1993**, *99*, 7983.
(31) Szalay, P. G.; Bartlett, R. J. *Chem. Phys. Lett.* **1993**, *214*, 481.
(32) Lischka, H.; Shepard, R.; Pitzer, R. M.; Shavitt, I.; Dallos, M.; Muller, T.; Szalay, P. G.; Seth, M.; Kedziora, G. S.; Yabushita, S.; Zhang, Z. *Phys. Chem. Chem. Phys.* **2001**, *3*, 664.
(33) Lischka, H.; Shepard, R.; Shavitt, I.; Pitzer, R. M.; Dallos, M.; Mueller, T.; Szalay, P. G.; Brown, F. B.; Ahlrichs, R.; Boehm, H. J.; Chang, A.; Comeau, D. C.; Gdanitz, R.; Dachsel, H.; Ehrhardt, C.; Ernzerhof, M.; Hoechtl, P.; Irle, S.; Kedziora, G.; Kovar, T.; Parasuk, V.; Pepper, M. J. M.; Scharf, P.; Schiffer, H.; Schindler, M.; Schueler, M.; Seth, M.; Stahlberg, E. A.; Zhao, J.-G.; Yabushita, S.; Zhang, Z.; Barbatti, M.; Matsika, S.; Schuurmann, M.; Yarkony, D. R.; Brozell, S. R.; Beck, E. V.; Blaudeau, J.-P. 2006, www.univie.ac.at/columbus.
(34) Shepard, R.; Shavitt, I.; Pitzer, R. M.; Comeau, D. C.; Pepper, M.; Lischka, H.; Szalay, P. G.; Ahlrichs, R.; Brown, F. B.; Zhao, J. G. *Int. J. Quantum Chem., Quantum Chem. Symp.* **1988**, *22*, 149.
(35) Shepard, R.; Lischka, H.; Szalay, P. G.; Kovar, T.; Ernzerhof, M. *J. Chem. Phys.* **1992**, *96*, 2085.
(36) Fonderie, V.; Maes, D.; Peeters, J. The kinetic coefficient of the ethylene + atomic oxygen reaction over extended pressure and temperature ranges. Department of Chemistry, Katholieke Universiteit Leuven: Louvain, Belgium, 1984.
(37) Baulch, D. L.; Cobos, C. J.; Cox, R. A.; Frank, P.; Hayman, G.; Just, T.; Kerr, J. A.; Murrells, T.; Pilling, M. J.; et al. *J. Phys. Chem. Ref. Data* **1994**, *23*, 847.
(38) Granucci, G.; Toniolo, A. *Chem. Phys. Lett.* **2000**, *325*, 79.

JP905070Z